Received 5 January 2018; revised 6 March 2018; accepted 9 March 2018. Date of publication 20 March 2018;
date of current version 31 August 2018. The review of this paper was arranged by Editor M. Nafría.

Digital Object Identifier 10.1109/JEDS.2018.2817286

SPICE Modeling of Photoelectric Effects in Silicon With Generalized Devices

CHIARA ROSSI [1], PIETRO BUCCELLA[1], CAMILLO STEFANUCCI[2], AND JEAN-MICHEL SALLESE[1]

1 Department of Electrical Engineering, École Polytechnique Fédérale de Lausanne, 1015 Lausanne, Switzerland
2 Image sensor solutions, AMS AG, 8640 Rapperswil, Switzerland

CORRESPONDING AUTHOR: C. ROSSI (e-mail: chiara.rossi@epfl.ch)

This work was supported by the Swiss National Science Foundation under Grant 200021_165773.

ABSTRACT Modeling photoelectric effects in semiconductors with electrical simulators is demonstrated in typical 1-D and 2-D architectures. The concept is based on a coarse meshing of the semiconductor with the so-called generalized lumped devices, where equivalent voltages and currents are used in place of minority carrier excess concentrations and minority carrier gradients, respectively, and where the light-induced excess carrier concentration in silicon is introduced by means of internal current sources. Generation, propagation, and collection of these minority carriers are analyzed for different structures which can behave as photosensors or solar cells. Both static and transient operations are found in good agreement with TCAD numerical simulations while using the same physical and geometrical parameters.

INDEX TERMS PN junction, modeling, SPICE, photocurrent, photo sensor, solar cell.

I. INTRODUCTION

A SPICE-compatible model used to simulate the injection and the propagation of excess carriers in the substrate of Smart Power ICs was developed in [1] and [2]. The corner stone of the concept was the definition of generalized lumped devices in which two additional external nodes were introduced to account for the excess in the minority carrier concentration and the excess in the minority carrier gradient through an equivalent voltage and an equivalent current respectively. In a second step, a network of the substrate made of these generalized devices is built according to the IC layout, leading to a circuit representation of the substrate that can be simulated with SPICE-like simulation software, thus including minority carriers parasitic coupling in the electrical simulation of the circuit [3].

Preliminary results including photogeneration of free carriers upon light absorption were presented at the ESSDERC 2017 conference [4]. The optically generated minority carriers were 'injected' by means of external voltage sources connected to the minority carrier nodes of the enhanced devices. The equivalent voltage was calculated so that the additional minority carrier density matches the density of photogenerated carriers. During the light pulse, the switch closes and settles the equivalent voltage on the minority carriers node, then returns to 'open' after the pulse. The distributed equivalent voltages (proportional to the excess carrier concentration) evolve according to the internal model of the generalized devices network. Space and time distributions of the carrier density and photocurrent were simulated for three relevant 1D semiconductor structures using a 1 ns light pulse at 600 nm wavelength. The results obtained were in good agreement with TCAD numerical simulations and the mismatch was as low as 2% without fitting parameters. However, the concept based on the external voltage sources is limited to the short pulse operation mode, and, when the light pulse is longer than the recombination time of the minority carriers, the external voltage will still fix the minority carrier density at a constant value, whereas a long charging process would change it gradually.

It is the aim of this work to extend the concept proposed in [4] for long pulse and DC operation. The models of the generalized lumped devices are thus modified so that the generation of minority carriers is now taken into account internally, embedded in the devices, without the need for any external voltage sources and switches. Based on this new feature, simulations of 1D and 2D structures are performed for DC and transient excitation. Additionally, the

model is used to predict the output characteristics of a basic solar cell.

II. PRINCIPLE OF GENERALIZED LUMPED DEVICES

A. CURRENT STATUS OF THE GENERALIZED LUMPED DEVICES

According to [2], simulation of minority carriers in a semiconductor layer involves three lumped elements: a generalized Diode, a generalized Homojunction and a generalized Resistor, as shown in Fig. 1.

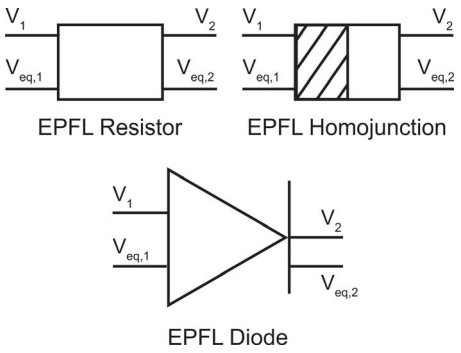

FIGURE 1. Generalized lumped devices (generalized Resistor, generalized Homojunction and generalized Diode) used for the SPICE-compatible simulation of minority carriers.

These devices are characterized by two additional nodes that propagate the information on the excess carrier density through equivalent voltages and currents. For instance, the diode can inject and collect carriers, the resistor is used to propagate them in the semiconductor, and the homojunction is used to account for discontinuities in the doping (of the same type) at the contact-semiconductor boundaries. The Finite Difference Method (FDM) is used to convert the set of drift-diffusion and continuity partial differential equations in a system of linear equations that can be mapped on a mesh [2]. This FDM gives rise to the so-called generalized lumped devices where the input and output variables are electrical quantities that can be solved by standard SPICE-like software. Solving the system of equations in the electrical domain will determine the local distribution of voltages and currents related to the space and time dependence of the majority and minority carriers.

In more details, each lumped device embeds two equivalent circuits: the Total Current Circuit (TCC) that accounts for currents and voltages, and the Minority Carrier Circuit (MCC) that holds for the minority carriers through the definition of an equivalent voltage V_{eq} proportional to the excess minority carrier concentration. Similarly, an equivalent current I_{eq} proportional to the minority carrier gradient is defined. In addition, the quasi-neutrality hypothesis is enforced, thus the excess majority carrier concentration equals the excess minority carrier concentration computed by the MCC. Combining TCC and MCC, a set of four terminals 'generalized' devices is obtained as reported in Fig. 1. These two circuits are coupled, especially in high injection [2] where the electric field adds a drift component to the minority carriers current, and where the injected carriers back modulate the conductivity of the substrate. Since the MCC and TCC are interrelated, variations in equivalent voltages and currents affect real voltages and real currents as well.

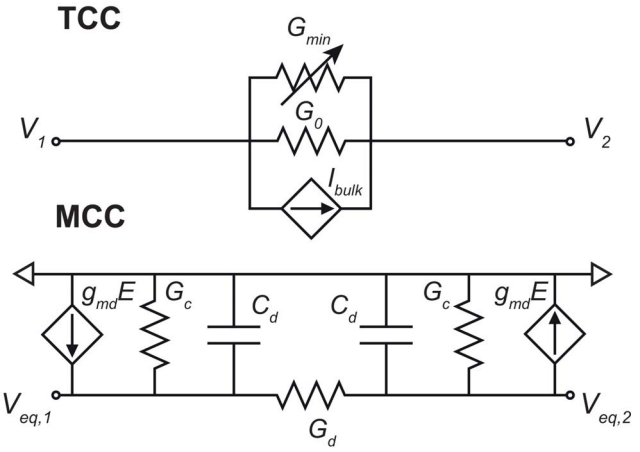

FIGURE 2. Schematic representation of the Total Current Circuit (TCC) and the Minority Carrier Circuit (MCC) for the generalized resistor case.

The TCC and MCC subcircuits for the generalized resistor are represented in Fig. 2. The generalized resistor, the simplest element, is the basic building block that is also used in the models for the generalized diode and homojunction. The TCC includes a constant resistance (G_0) which represents the standard doping dependent resistance of the substrate, a variable resistance (G_{min}) that takes into account the modulation of the conductivity due to the excess minority carriers, and a current source (I_{bulk}) which is a correction term used to model the difference between majority and minority diffusion currents. In addition, the MCC includes a conductance (G_d) depending on the diffusivity that regulates the diffusion current, and a conductance (G_c) depending on the electron-hole pairs lifetime (Shockley–Read–Hall model) that regulates the minority carriers recombination in the discretized volume. Finally, drift is also present in the MCC through current sources ($g_{md}E$) depending on the potential drop. Importantly, diffusion capacitances (C_d) are also implemented, see [5] for a more in depth analysis.

B. GENERALIZED LUMPED DEVICES WITH PHOTOELECTRIC EFFECTS

The models for the generalized lumped devices developed in [2] are extended to consider photoelectric effects. A new continuity equation including photogenerated carriers is discretized using the FDM and gives rise to a new component in the MCC circuit, i.e., a current source (I_G), drawn in red in Fig. 3. The current holds for the electron-hole pairs generation rate (G), which is proportional to the density of photons absorbed per unit time. This generation rate is given by:

$$G = \frac{\alpha \lambda}{hc} I \tag{1}$$

where α is the absorption coefficient, λ is the photon wavelength, h is the Planck constant, c is the speed of light and I is the light intensity inside the semiconductor following the Beer-Lambert law $I(x) = I_0 \exp(-\alpha x)$.

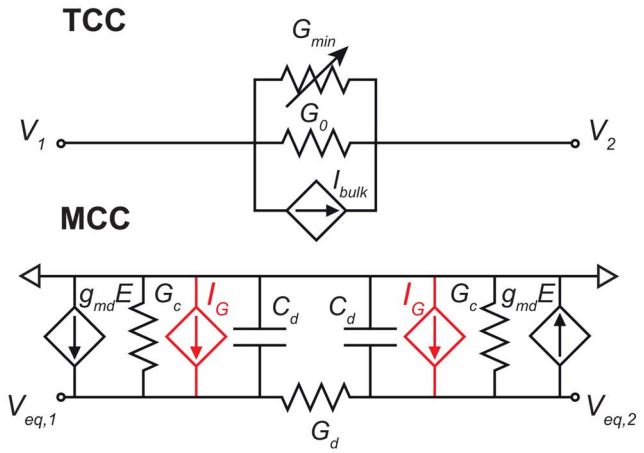

FIGURE 3. Schematic representation of the Total Current Circuit (TCC) and the Minority Carrier Circuit (MCC) for the generalized resistor case including photoelectric effects.

III. MODELING CHARGES AND PHOTOCURRENT IN 1D STRUCTURES

Generation, recombination and propagation of carriers upon a pulse of light are studied in a p-doped ($N_a = 10^{16}$ cm^{-3}) silicon resistor of 20 μm length, 5 μm wide and 1 μm thick. Three different structures have been considered, each of which introduces different categories of generalized elements:

S1: Electrodes are in direct contact with the p-type silicon (Ohmic contact conditions are imposed).

S2: Electrodes are contacting two highly-doped layers ($Na = 2 \cdot 10^{19}$ cm^{-3}) of 0.1 μm thickness, which constitute two homojunctions.

S3: A reverse-biased diode terminates the resistor (note that two homojunctions are introduced as well, $N_{a/d} = 2 \cdot 10^{19}$ cm^{-3}).

All devices are illuminated uniformly from one side with a 1 ns light pulse of 10^3 W/cm^2 at a wavelength of 600 nm (the absorption coefficient α at 600 nm is $4.14 \cdot 10^3$ cm^{-1} for silicon) and the current is computed between the two sided contacts (note that this kind of experiment was used to measure carriers mobility in semiconductors [6], [7] with structures such as S1).

Fig. 4 is the layout of the structure S3 with the different zones highlighted, and where the equivalent network made of generalized lumped devices (generalized homojunctions, resistors and diodes) is superimposed. Since illumination is uniform, a simple 1D discretization scheme is used. A similar decomposition is adopted for S1 and S2. The number of lumped elements is essentially imposed by the mesh density needed for an accurate evaluation of the mean optical generation rate contained in the volume between the nodes. In order to minimize the number of components, still keeping the mismatch with numerical simulations below 2%, eight mesh nodes are placed along the illuminated zone, namely at x = 0.5 μm, 1 μm, 2 μm, 3 μm, 4 μm, 5 μm, 6 μm and 8 μm. As soon as the generation of free carriers becomes negligible (when $x > 4\alpha^{-1} \sim 8$ μm), a simple generalized resistance is sufficient to account for drift, diffusion and recombination mechanisms, thus neglecting optical generation. However, in order to extract the excess carrier density with respect to space and time, additional lumped components are intentionally introduced.

TCAD simulations are run for each structure imposing a doping-dependent mobility law and the Shockley-Read-Hall recombination model. Light excitation is defined as a time dependent monochromatic flux. Importantly, the same physical parameters as for TCAD simulations are used for the generalized devices, i.e., no fitting parameter is introduced in the generalized devices models for S1, S2 and S3.

In the following paragraphs, simulations using the lumped devices model and the TCAD software are presented for the structures S1, S2 and S3.

A. UNIFORMLY P-TYPE DOPED SILICON

The device S1 consists of a uniformly p-doped silicon layer with a doping density of 10^{16} cm^{-3}. Ideal contacts are defined at x = 0 μm and x = 20 μm, meaning that full recombination of excess minority carriers is imposed at these interfaces. The resistor is biased with a DC voltage of 0.5 V applied on the illuminated side. The densities of electrons (minority carriers) at different coordinates obtained from SPICE and TCAD simulations are plotted in Fig. 5. Continuous lines represent the lumped elements model while

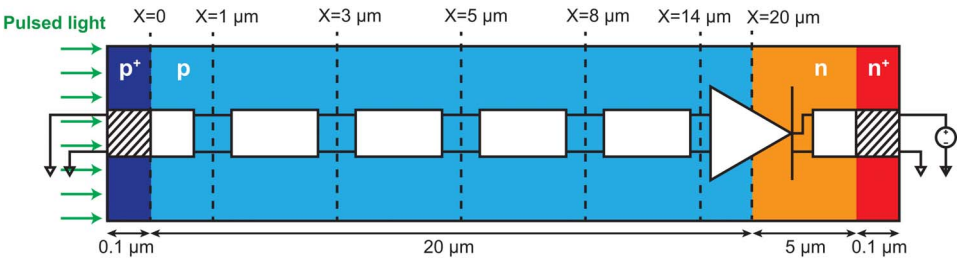

FIGURE 4. Structure S3: layout and equivalent network of generalized lumped devices (generalized homojunctions, resistors and diodes). The structure is uniformly illuminated from the left side justifying a 1D discretization scheme.

symbols are for TCAD. The origin of time is set after the pulse of light, i.e., after 1 ns.

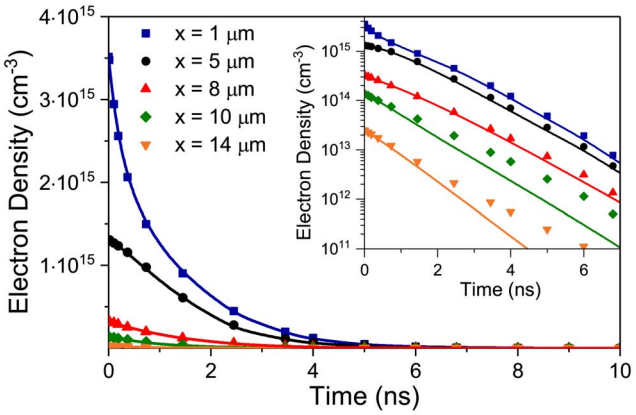

FIGURE 5. Simulated electron density for the structure S1 (continuous line for model and symbols for TCAD). The inset shows the electron density in logarithmic scale.

Fig. 5 shows that the excess minority carrier concentrations decay about 6 ns after the light pulse, as electrons are accelerated by the electric field and collected rapidly. Beyond 8 μm, the electron density becomes negligible. The equivalent SPICE model is in good agreement with numerical simulations. The lumped modeling scheme can thus predict the time dependence of the minority carrier concentration between the contacts. Concerning the photocurrent (difference between the total current and the dark current) at the output, SPICE simulations are still accurate, see Fig. 6. Note that the free carrier density is about one order of magnitude lower than the doping, meaning that moderate injection conditions are satisfied.

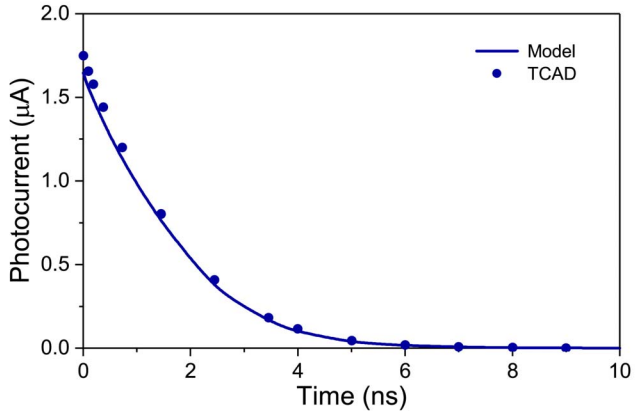

FIGURE 6. Simulated photocurrent, i.e., total current minus dark current, for the structure S1 (continuous line for model and symbols for TCAD).

B. P-TYPE DOPED SILICON WITH HIGHLY DOPED HOMOJUNCTIONS

In the structure S2, highly p-type doped regions ($2 \cdot 10^{19}$ cm^{-3}) are implemented at x = 0 μm and at x = 20 μm

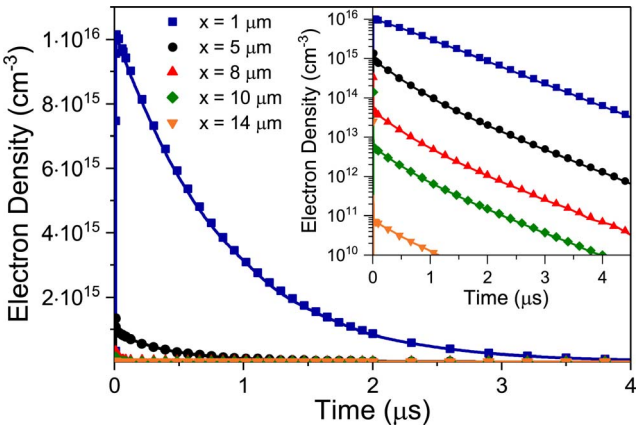

FIGURE 7. Simulated electron density for the structure S2 (continuous line for model and symbols for TCAD). The inset shows the electron density in logarithmic scale.

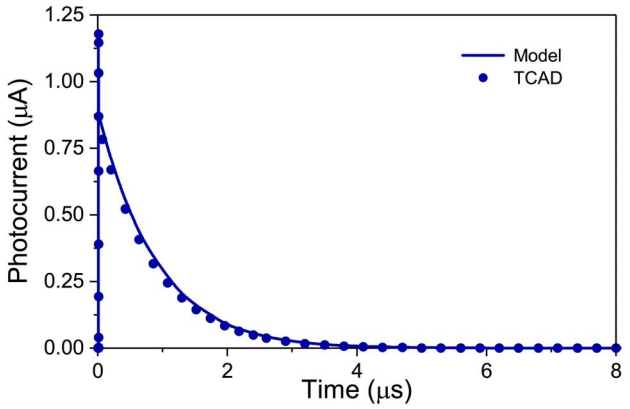

FIGURE 8. Simulated photocurrent, i.e., total current minus dark current, for the structure S2 (continuous line for model and symbols for TCAD).

to create Ohmic contacts. These highly-doped layers have a negligible extension of 0.1 μm. The structure is still biased with a DC voltage of 0.5 V applied on the illuminated side. Fig. 7 plots the electron density versus time at different coordinates obtained with the generalized devices and with numerical TCAD simulations. Again, there is a good agreement between these two approaches. It is worth to note that whereas the pulse of light is the same for S2 and S1, the density of minority carriers is about one order of magnitude higher in S2 compared to S1, i.e., 10^{16} instead of 10^{15} cm^{-3}, and the time scale is in the μs range for S2 instead of some tens of ns, as for S1. Similarly, the transient current decays in the μs range (see Fig. 8), which indicates that the drift towards the electrical contact is no longer the dominant mechanism. In fact, the additional homojunctions exert a repelling effect on minority carriers due to the barrier created by the doping gradient. Thus, electrons cannot be collected effectively by the contact and they remain longer inside the silicon. Excess of holes could be collected at the counter electrode as they face no barrier, but, since

propagation of photogenerated e/h pairs is driven by ambipolar transport, holes move with electrons as a whole. Note that also these fine points are accurately depicted by the equivalent generalized circuit.

C. RESISTANCE WITH REVERSE-BIASED PN JUNCTION

The last structure investigated (S3) consists of a diode in series with a uniformly doped silicon layer, as represented in Fig. 4. The p-type layer has a length of 20 μm and the n-type layer of 5 μm. Highly doped p and n regions are also included for Ohmic contacts (both with a length of 0.1 μm). In this case a DC voltage of 0.5 V is applied to the n-doped (non-illuminated) side to set the diode in reverse mode. Again, the electron density in transient mode at different coordinates is well predicted by the lumped device approach in Fig. 9. The transient current is plotted in Fig. 10 and, as for the minority carrier concentrations, the correspondence between numerical TCAD simulations and the predictions of SPICE simulations is reasonable. The overall kinetic for S3 is mid-way between S1 and S2. Since the potential drops almost entirely across the pn junction, the dominant mechanism in this case is diffusion.

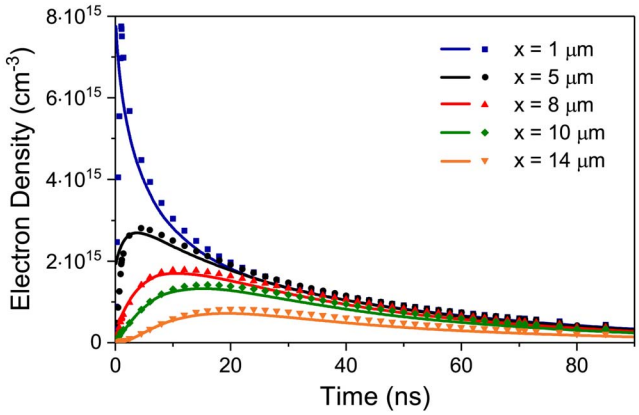

FIGURE 9. Simulated electron density for the structure S3 (continuous line for model and symbols for TCAD).

This is supported by the photocurrent which almost vanishes after about 150 ns, i.e., the typical time needed for electrons to diffuse from the surface to the pn junction at $x = 20$ μm. The excess in the electron density simulated at coordinates where there is no light generation ($x \geq 8$ μm) is initially negligible ($t = 0$), then it shows a maximum after some tens of ns (this value increases when moving further from the surface). This behavior is consistent with a diffusion process where the cloud of carriers photogenerated at the surface at time zero moves towards the pn junction with time. Again, the lumped modeling approach captures these processes accurately.

It is interesting to increase the intensity of light from 10^3 W/cm^2 to 10^4 W/cm^2 to investigate high injection regime. Simulations confirm that for 10^4 W/cm^2 the density of the photogenerated carriers is higher than the doping concentration (the electron density reaches $\sim 10^{17}$ cm^{-3} at the left homojunction interface). Fig. 10 shows the photocurrent for moderate (10^3 W/cm^2) and high (10^4 W/cm^2) injection conditions for S3. The effect of high injection degrades slightly the matching with TCAD, but the agreement is still acceptable. We also state (not reported here) that the lumped model is accurate in high injection for the structure S1, while it degrades significantly for S2 where the relative error is about 15%. In fact, the model can cope with high injection for cases S1 and S3 because the minority carrier concentration goes back to steady state in a quite short time, while for case S2 the concentration remains greater than the doping concentration longer, leading to bigger errors.

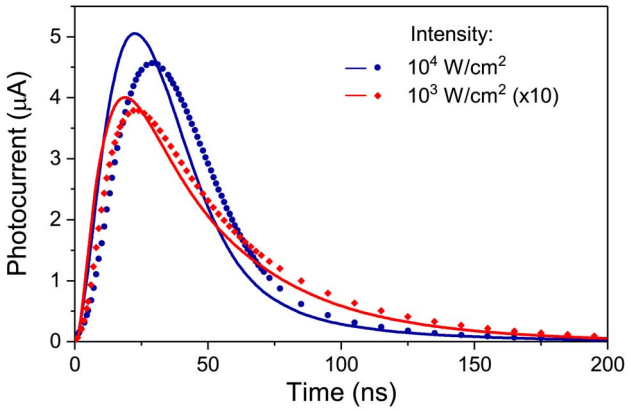

FIGURE 10. Simulated photocurrent collected by the reverse-biased diode in S3 for two light pulse power densities (continuous line for model and symbols for TCAD). In the 10^3 W/cm^2 case, the photocurrent values have been multiplied by a factor of 10.

IV. MODELING CHARGES AND PHOTOCURRENT IN 2D STRUCTURES

The analysis carried out in specific 1D systems is now generalized to simulate photoelectric effects in a 2D photodiode, represented in Fig. 11 where the different doping regions are highlighted. The equivalent generalized devices network superimposed is only aimed at illustrating what such network looks like. The diode consists of a n-type region (40 μm wide and 10 μm thick, the default value is 1 μm in the third dimension) with doping concentration of $2 \cdot 10^{16}$ cm^{-3} surrounded by a p-type region (100 μm wide, 20 μm thick) with doping concentration of $4 \cdot 10^{15}$ cm^{-3}, both contacted with highly doped regions (doping of $2 \cdot 10^{19}$ cm^{-3}, 5 μm wide, 0.25 μm thick).

The structure is illuminated from the top with a wavelength of 600 nm and the intensity is assumed constant along the x-axis. The substrate network mesh is set to 0.5 μm in the y direction where photogeneration takes place, so to minimize the error in the linearization of the exponential characteristic of light absorption. Along the x-axis, the mesh size is dictated by the layout of the structure and therefore can be relaxed with respect to the y direction. Further details on the mesh optimization will be discussed later. As in the previous section, TCAD simulations are run to validate the model and

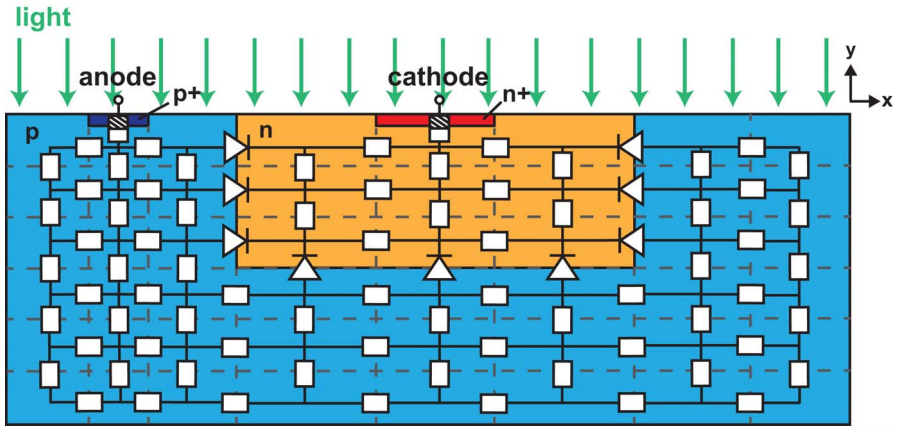

FIGURE 11. Sketch of the layout of the diode structure used for 2D simulations. The grey dotted lines symbolize the mesh. The equivalent network of the generalized lumped devices is superimposed. The structure is illuminated from the top and the light intensity is constant along the x-axis.

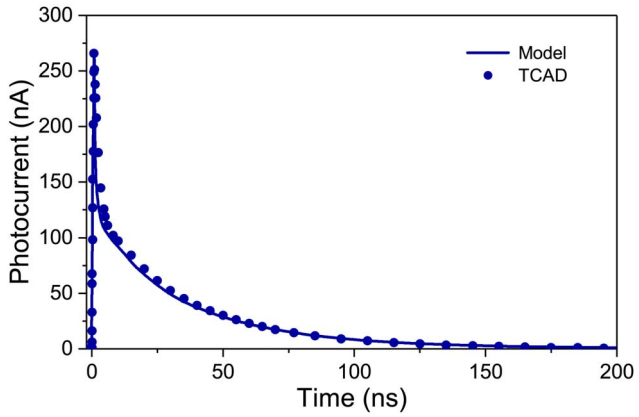

FIGURE 12. Photocurrent collected by the 2D diode in reverse mode when illuminated with a single pulse of light (continuous line for model and symbols for TCAD).

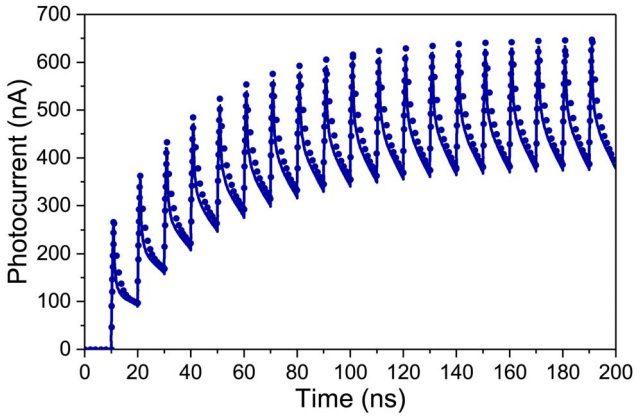

FIGURE 13. Photocurrent collected by the 2D diode in reverse mode when illuminated with periodic pulses (continuous line for model and symbols for TCAD).

the same physical parameters as for TCAD simulations are used in the analytical models of lumped devices. The output characteristics are simulated either under pulsed or constant illumination.

A. TRANSIENT OPERATION

A.1. PULSED ILLUMINATION

The structure in Fig. 11 is illuminated with a single pulse of light of 1 ns with an intensity of 10 W/cm^2. The photocurrent collected by the diode biased in reverse mode is plotted as a function of time in Fig. 12. As for the 1D case, the results obtained with the equivalent network (continuous line) fit well the data obtained with TCAD numerical simulation (symbols). The model correctly simulates both the quick rising of the photocurrent during the light pulse and the decreasing phase after the pulse, before vanishing around 200 ns. The time response of the photodiode can thus be predicted with circuit simulators, within milliseconds range simulation times.

A.2. PERIODIC EXCITATION

The same structure sets in reverse bias is now illuminated with periodic pulses of 1 ns duration every 10 ns, while the light intensity is still 10 W/cm^2. The simulations performed using the lumped devices model and TCAD tool are reported in Fig. 13. Even for this mode of operation, the model predicts accurately the time dependence of the photocurrent. Both the transient waveform at early times as well as the overall envelope are well tracked. In particular, the model simulates the evolution of the charge density and related current inside the structure without degrading the accuracy, i.e., without accumulating errors. For instance, the variation in photocurrent between each pulse is always well estimated (i.e., around 260 nA). Therefore, the sensitivity and the bandwidth of photodetectors can be computed relying on this equivalent network. The optimization of the layout to target some characteristics can be performed using circuit simulators without the need to build a compact model of the photoelectric element, a key feature to optimize the sensor *and* its control/sensing circuitry before any fine tuning.

B. DC OPERATION

In addition to transient operation, the DC characteristic is investigated by exciting the device in Fig. 11 with a constant flux of photons. In addition, a resistive load is used to interconnect the anode with the cathode in order to simulate a solar cell. The value of the external resistance is ramped gradually to rebuild the complete I-V characteristic, plotted in Fig. 14 and Fig. 15 for different light intensities (note that a power density of 0.1 W/cm^2 corresponds to the typical value of the sun intensity at sea level at zenith and this intensity is used to characterize solar cells).

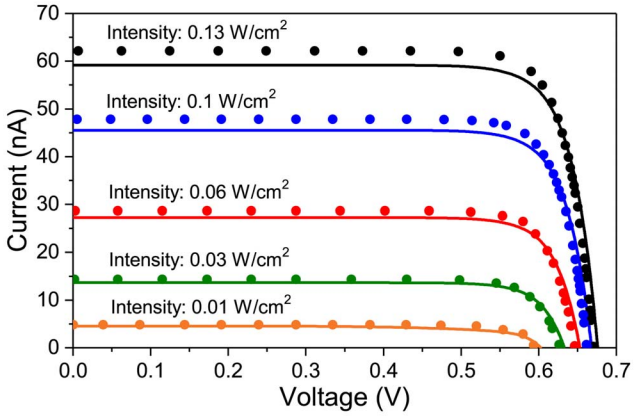

FIGURE 14. I-V characteristics of the 2D diode for different light intensities (DC operation). This simulates the operation of a simple solar cell (continuous line for model and symbols for TCAD).

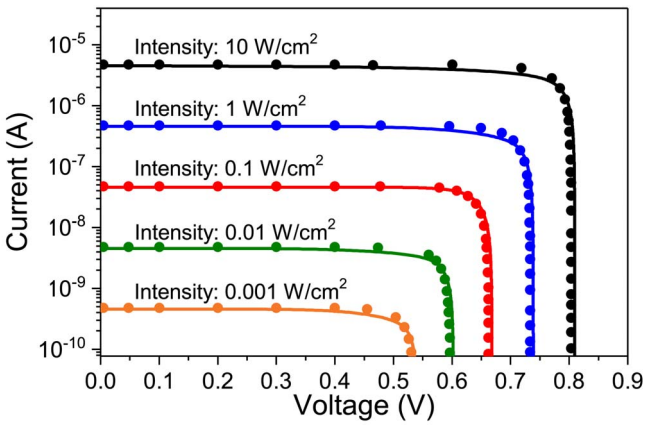

FIGURE 15. I-V characteristics of the 2D diode for different light intensities (DC operation). The intensity is ranged over several orders of magnitude. This simulates the operation of a simple solar cell (continuous line for model and symbols for TCAD).

The simulation performed with the lumped devices network (continuous line) is in good agreement with TCAD (symbols) for all intensities of light. The whole characteristic, including the open circuit voltage and the short circuit current, are well estimated. This is a key feature that arises from the intimate coupling between the TCC and MCC subcircuits in generalized lumped devices (see the Appendix for more details). The open circuit voltage reported in Fig. 14 and Fig. 15 is predicted with less than 1% error with respect to TCAD, while the error in predicting the short circuit current is a bit larger, but still less than 5% ($\sim$ 4.8%). Those values are quite accurate given that no fitting parameters have been introduced. Since the full I-V characteristic can be simulated, the maximum output power of the solar cell can be estimated from the technological cross section and without the need of an analytical model of the whole device.

This kind of simulation is now used to assess mesh optimization. To this purpose, a continuous illumination with a light intensity constant along x of 0.1 W/cm^2 is adopted, and the mesh is changed independently along x and y axis. Regarding the mesh size along the y-direction, two different values are used: a low value where the absorption of light is effective, and a larger one where photogeneration is negligible. We propose to set the boundary between these two regions at four times the absorption length (i.e., $4\alpha^{-1}$, which depends on the wavelength). Simulations of different structures (not presented here) show that the mesh size where the photogeneration is negligible should be at the most one fifth of the diffusion length of the minority carriers. This criterion will also be adopted when meshing the x-direction.

The optimization of the mesh in presence of photogeneration ($y < 4\alpha^{-1}$) is now shown in Fig. 16. As mentioned before, the mesh size is set to one fifth of the diffusion length for $y > 4\alpha^{-1}$. When the mesh size is decreased in the region with photogeneration ($y < 4\alpha^{-1}$), the model gets closer to the numerical simulations, but an asymptote is reached for steps below 0.5 μm, i.e., about one fifth of the absorption length (i.e., α^{-1}).

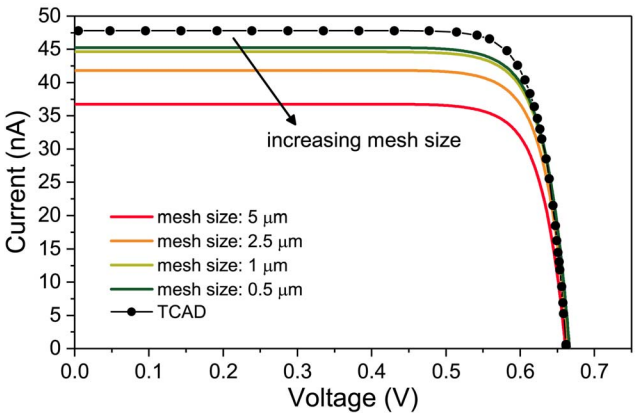

FIGURE 16. I-V characteristics of the 2D diode in solar cell operation for different mesh sizes are compared with the TCAD results. Results for mesh sizes smaller than 0.5 μm are not shown as the accuracy does not increase anymore and the same characteristics as the 0.5 μm case are found. This mesh optimization is performed using a light intensity of 0.1 W/cm^2.

Even though mesh optimization is not the aim of this work, this simple analysis reveals that a rule of thumb can be proposed as follows: the mesh size should be one fifth of the diffusion length when photogeneration is negligible, or one fifth of the absorption length of the light (i.e., α^{-1})

for regions where light absorption impacts the free carrier concentration.

V. CONCLUSION

A SPICE-compatible model developed for substrate coupling in Smart Power ICs was adapted to simulate generation, propagation and collection of photocarriers in different semiconductor structures. Good agreement was obtained between TCAD and SPICE-based simulations. It comes out that the generalized elements arranged in a lumped topology can predict the behavior of excess carrier concentrations without the need for any fitting parameters. It was shown that this approach is suitable to evaluate some basic performances of optoelectronic devices both in DC and transient operation. In particular, the complete I-V characteristic of a solar cell, including the open circuit voltage and short circuit current, as well as the frequency response of a photodetector were accurately predicted. In addition to the advantages brought by the co-simulation of the photodiode with IC's active devices, this approach can be used as a fast pre-optimization tool before fine tuning with numerical TCAD simulations. This work is a first step towards optoelectronics simulations based on generalized elements with standard circuits simulation tools.

APPENDIX

This Appendix highlights the link between the generalized diode model and photoelectric effects, and explains how the generalized devices (including photogeneration) can simulate a simple solar cell, for instance.

The schematic represented in Fig. 17 is the circuital equivalence of the generalized diode model. It consists of an equivalent circuit of a p-type and n-type resistors, which model the two neutral region of the diode, and three dependent sources that model the pn junction. We restrict the analysis to low injection conditions (excess carrier concentration negligible with respect to the doping) for which the model can be simplified by neglecting the components G_{min}, I_{bulk}, $g_{md}E$ (these are correction terms for high injection). Moreover, to further simplify the analysis, steady-state condition are considered, i.e., no capacitances, and the drift of excess carriers in the neutral regions is neglected, thus discarding the internal resistance as well. These dummy components are marked in grey color in Fig. 17.

The voltage sources in the MCC (V_n and V_p) model the excess minority carrier concentrations at the boundary of the space-charge region according to the pn junction law [7]:

$$V_n = qn_{p0}\left(e^{\frac{V_j}{V_t}} - 1\right) \tag{A1}$$

$$V_p = qp_{n0}\left(e^{\frac{V_j}{V_t}} - 1\right) \tag{A2}$$

where n_{p0} and p_{n0} are the equilibrium minority carrier densities, V_j is the voltage drop on the space-charge region, V_t is the thermal voltage, and q is the electron charge used as scaling factor to transform excess carrier concentrations into voltages. Regarding the current source I_{tot} in the TCC, in low injection its value is proportional to the gradient of the minority carriers, which is given by the current flowing in the diffusion resistances G_{dn} and G_{dp} in the MCC:

$$I_{tot} = \left(V_{eq,1} - V_n\right) G_{dn} + \left(V_{eq,2} - V_p\right) G_{dp} + I_{rec} \tag{A3}$$

where I_{rec} is the current contribution coming from generation recombination processes in depletion region (Sah-Noyce-Shockley) [2].

These three dependent sources couple the MCC and the TCC: the voltage drop across the diode, the excess carrier concentrations and gradients are all interrelated, thanks to (A1), (A2), and (A3). If there is no generation and a potential is applied externally to the diode, V_n and V_p are imposed by (A1) and (A2) while the current is given by (A3) according to V_n and V_p and the resistances of the equivalent network that set $V_{eq,1}$ and $V_{eq,2}$ (note that the diode is connected with generalized resistors in the network). When the diode is illuminated, the values of $V_{eq,1}$ and $V_{eq,2}$ result from the steady-state condition involving generation and recombination of excess carriers (which depend on the whole network of generalized resistors and diodes).

We now discuss the open circuit voltage and short current circuit of the diode under illumination.

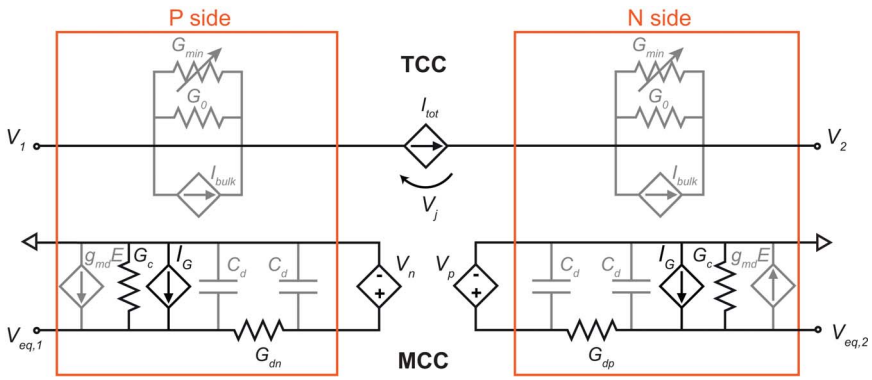

FIGURE 17. Schematic representation of the Total Current Circuit (TCC) and the Minority Carrier Circuit (MCC) for the generalized diode. The components in grey color are negligible for steady-state and low injection conditions.

The open voltage roots in the equivalent voltages $V_{eq,1}$ and $V_{eq,2}$. These arise from the current, originating by the generation current sources (I_G), that flows in the recombination resistances G_c. More precisely, in open circuit condition, the total current I_{tot} is zero and, according to (A3), neglecting I_{rec}, also the currents flowing in the resistances G_{dn} and G_{dp} are equal to zero, since these diffusion currents should have the same sign. It implies that V_n and V_p are necessarily equal to $V_{eq,1}$ and $V_{eq,2}$. Equations (A1) and (A2), thus, link directly $V_{eq,1}$ and $V_{eq,2}$ with the voltage drop on the diode, i.e., V_j (the simulator will search for the solution that satisfies all the relations). As expected, a logarithmic relationship between the open circuit voltage (V_j in this case) and the excess carrier density (proportional to $V_{eq,1}$ and $V_{eq,2}$) is found.

In short circuit conditions, the applied voltage is zero and thus V_n and V_p reach their minimal values. Since $V_{eq,1}$ and $V_{eq,2}$ are fixed by the rest of the circuit, I_{tot} is maximum, as confirmed in Fig. 14 and Fig. 15.

In between, the equivalent circuit can model the intermediate regime quite accurately.

REFERENCES

[1] F. Lo Conte, J.-M. Sallese, M. Pastre, F. Krummenacher, and M. Kayal, "Global modeling strategy of parasitic coupled currents induced by minority-carrier propagation in semiconductor substrates," *IEEE Trans. Electron Devices*, vol. 57, no. 1, pp. 263–272, Jan. 2010, doi: 10.1109/TED.2009.2035025.

[2] C. Stefanucci, P. Buccella, M. Kayal, and J.-M. Sallese, "Spice-compatible modeling of high injection and propagation of minority carriers in the substrate of smart power ICs," *Solid State Electron.*, vol. 105, pp. 21–29, Mar. 2015, doi: 10.1016/j.sse.2014.11.016.

[3] P. Buccella *et al.*, "Methodology for 3-D substrate network extraction for spice simulation of parasitic currents in smart power ICs," *IEEE Trans. Comput.-Aided Design Integr. Circuits Syst.*, vol. 35, no. 9, pp. 1489–1502, Sep. 2016, doi: 10.1109/TCAD.2015.2513008.

[4] C. Rossi, P. Buccella, C. Stefanucci, and J.-M. Sallese, "SPICE modeling of light induced current in silicon with 'generalized' lumped devices," in *Proc. 47th Eur. Solid-State Device Res. Conf. (ESSDERC)*, Leuven, Belgium, 2017, pp. 26–29, doi: 10.1109/ESSDERC.2017.8066583.

[5] C. Stefanucci, P. Buccella, M. Kayal, and J.-M. Sallese, "Modeling minority carriers related capacitive effects for transient substrate currents in smart power ICs," *IEEE Trans. Electron Devices*, vol. 62, no. 4, pp. 1215–1222, Apr. 2015, doi: 10.1109/TED.2015.2397394.

[6] J. R. Haynes and W. Shockley, "The mobility and life of injected holes and electrons in germanium," *Phys. Rev.*, vol. 81, no. 5, pp. 835–843, 1951, doi: 10.1103/PhysRev.81.835.

[7] S. M. Sze, *Physics of Semiconductor Devices*, 2nd ed. New York, NY, USA: Wiley, 1981, doi: 10.1002/0470068329.

CHIARA ROSSI received the M.Sc. degree in micro and nano technologies for integrated systems in 2016 from École Polytechnique Fédérale de Lausanne (EPFL), Switzerland, Institut National Polytechnique de Grenoble, France, and Politecnico di Torino, Italy. In 2016, she joined the Group of Electron Device Modeling and Technology, EPFL, where she is currently pursuing the Ph.D. degree working on modeling of radiation effects in integrated circuits.

PIETRO BUCCELLA received the M.Sc. degree in electronic engineering from the Polytechnic University of Turin, Italy, in 2005 and the Ph.D. degree in microsystems and microelectronics from EPFL, Lausanne, Switzerland, in 2016, where he is a Post-Doctoral Researcher. From 2005 to 2010, he was an Analog IC Design Engineer with Microchip Technology Switzerland working in the field of sensor interface, high-voltage, and power management CMOS integrated circuit design. From 2010 to 2012, he was a Security Engineer with Kudelski Group, testing the hardware security of microcontroller and smartcard chips. His main research interests include sensor interface, power management, and mixed-signal HV IC design.

CAMILLO STEFANUCCI received the joint M.Sc. degree in nanotechnologies from the Polytechnic University of Turin, Italy, and the Institut National Polytechnique de Grenoble, France, in 2011, the M.Sc. degree in electronics engineering from the Polytechnic University of Milan, Italy, in 2012, and the Ph.D. degree in microelectronics from École Polytechnique Fédérale de Lausanne, Switzerland, in 2016. As an affiliated research scientist of EPFL, he is author of several publications on minority carrier's substrate modeling for HVCMOS circuits. He has experience as Analog IC Designer with the Swiss Center of Microelectronics and AMS AG, where he is currently developing industrial ASICs. His research and technical interests include latch-up modeling, power management circuits, HV analog design, and data converters.

JEAN-MICHEL SALLESE received the Ph.D. degree in physics from the University of Nice-Sophia Antipolis. He joined the École Polytechnique Fédérale de Lausanne and was appointed as a Maître d'Enseignement et de Recherche. His current research concerns modeling of emerging electron devices and he currently gives lectures on modeling electron devices and semiconductor technology.